Biointerface Research in Applied Chemistry
Platinum Open Access Journal (ISSN: 2069-5837)

Article
Volume 11, Issue 6, 2021, 14316 - 14335
https://doi.org/10.33263/BRIAC116.1431614335

Palladium Complexes Based on 2-Hydrazinopyridine Ligand: Synthesis, Spectroscopic Studies, DFT Calculations, and Cytotoxicity

Sattar R. Majeed [1], Mina A. Amin [2], Fawzy A. Attaby [3], Ahmed A. Soliman [4,*]

[1] Department of Chemistry, College of Science, University of Anbar, Ramadi, Anbar, Iraq; sc.sat70tar@uoanbar.edu.iq (S.R.M);
[2] Department of Chemistry, Faculty of Science, Cairo University, 12613 Giza, Egypt; mina_anis89@hotmail.com (M.A.A.);
[3] Department of Chemistry, Faculty of Science, Cairo University, 12613 Giza, Egypt; fattaby@gmail.com (F.A.A);
[4] Department of Chemistry, Faculty of Science, Cairo University, 12613 Giza, Egypt; ahmedsoliman61@gmail.com (A.A.S);
* Correspondence: ahmedsoliman61@gmail.com;

Scopus Author ID 55574193552

Received: 3.02.2021; Revised: 28.02.2021; Accepted: 2.03.2021; Published: 10.03.2021

Abstract: Three new palladium complexes based on 2-hydrazinopyridine (hzpy) ligand, coupled with oxalate (ox), malonate (ma) and pyrophosphate (pyph) ligands, were prepared; [Pd(hzpy)(ox)], [Pd(hzpy)(ma)] and [Pd(hzpy)(pyph)]. The spectroscopic and thermal studies of the complexes suggested that the complexes were of square planar geometry. The complexes were thermally stable with an overall activation energy of 678, 981, and 633 kJ mol–1 for [Pd(hzpy)(ox)]. [Pd(hzpy)(ma)] and [Pd(hzpy)(pyph)], respectively. Geometric optimization of the three complexes was performed at DFT/B3LYP/SDD level through Gaussian 09. TDDFT and frequency calculations were studied to investigate the electronic and vibrational transitions. The potential *in vitro* cytotoxic activities of the three complexes was studied. The complexes exhibited a moderate cytotoxic effect against four cancer cell lines; MCF-7 (human breast cancer cell line), HepG-2 (human Hepatocellular carcinoma), PC-3 cells (human prostate carcinoma), and HEP-2 (Larynx carcinoma). The IC50 values of the three complexes exhibited a good performance against PC-3 cell line with low IC50 values reached 2.87 µg/ml for [Pd(hzpy)(ox)] compared to the IC50 of Vinblastine sulfate (42.4 µg/ml).

Keywords: palladium complex; dinitrogen ligands; cytotoxicity; DFT.

Abbreviations:

TGA	Thermal gravimetric analysis
DFT	Density functional theory
TD-DFT	Time-dependent density functional theory
LLCT	Ligand-ligand charge transfer
MLCT	Metal-ligand charge transfer
ΔE	Energy gap
χ	Absolute electronegativity
η	Absolute hardness
σ	absolute softness
Pi	chemical potentials
ω	global electrophilicity
S	global softness
ΔN_{max}	Additional electronic charge

1. Introduction

Coordination chemistry supported humans with many metal complexes used for different purposes, including catalysis and biological applications (antitumor drugs) [1]. The importance of these applications paved the way to improve and tune the chemical properties of the metal complexes and the accompanying ligands. Cisplatin, carboplatin and oxaliplatin are the main platinum-based compounds used as antitumor agents [2, 3]. Unfortunately, cis-platin, the main antitumor agent, acquired resistance and has toxic effects. Such resistance and toxicity forced researchers to direct their efforts for preparing analogs to cisplatin [4, 5]. The similar properties (structural and thermodynamic) between platinum and palladium (soft Lewis acids) encourage the researchers to prepare new palladium-based analogs to be used as antitumor agents to avoid cisplatin drawbacks [6]. Palladium-based coordinated compounds have higher activity compared to that of the platinum alternatives as they hydrolyze rapidly. The palladium complexes' fast kinetics form reactive spices within the biological systems that cannot reach their targets [7-9]. The ligands' type and nature are critical in tuning the reactivity, stability, and lipophilicity of the metal complexes [10]. The palladium complexes' reactivity requires a smart design for the complexes to stabilize complexes such as using bulky, chelating, and nitrogen-based ligands such as pyridine derivatives imidazole and 1,10-phenanthroline [11-14]. Modifying the coordinated ligands to the palladium center can also tune and enhance the palladium complexes' cytotoxic activities [15-20]. The pyridine derivative-based complexes were reported to act as antitumor agents, and the ability of their palladium complexes proved their ability to interact with DNA [21, 22]. We continue our research on Pd(II) complexes in the current work, soluble in water, based on 2-hydrazinopyridine ligand with potential antitumor activities. The three palladium complexes' water solubilities were enhanced by coordinating the palladium center ion with oxalate, malonate, and pyrophosphate ligands. The *in vitro* cytotoxic activities of the palladium complexes were investigated against four cancer cell lines; MCF-7 (human breast cancer cell line), HepG-2 (human Hepatocellular carcinoma), PC-3 cells (human prostate carcinoma), and HEP-2 (Larynx carcinoma), and the IC50 values were recorded. Three palladium complexes were synthesized and characterized using spectroscopic techniques (IR, UV, and NMR) magnetic and thermal analyses. The complexes were optimized at DFT/B3LYP/SDD level.

2. Materials and Methods

2.1. Materials.

Sodium tetrachloro palladate, sodium pyrophosphate, 2-hydrazinopyridine hydrochloride, malonic acid, and oxalic acid were obtained from Sigma Aldrich.

2.2. Physical measurements.

The absorption spectra were collected using an Optizen UV–Vis spectrophotometer. The IR spectra were recorded using a Jasco FT-IR – 460 plus. Varian-Oxford Mercury VX-300 NMR (300 MHz) spectrometer was used for ^{1}HNMR spectra (DMSO-d_6). FAB-MS measurements of the compounds were performed via JEOL JMS- AX 500 spectrometer. TGA analyses of the three complexes were performed by Shimadzu thermogravimetric analyzer (TGA-50H) under a continuous flow of N_2 and heating rate of 10 ^{o}C / min.

2.3. Theoretical calculations.

The geometrical optimization of the palladium complexes (Figures 1 – 3) in the gas phase was performed at DFT/B3LYP/SDD level [23-27] using GAUSSIAN 09 [28]. The output files were displayed using GaussView 5.0. The frequency and TD-DFT calculations were also investigated. The bond angles and lengths around the metal center are listed in Tables S1 - S3 (Supplementary materials).

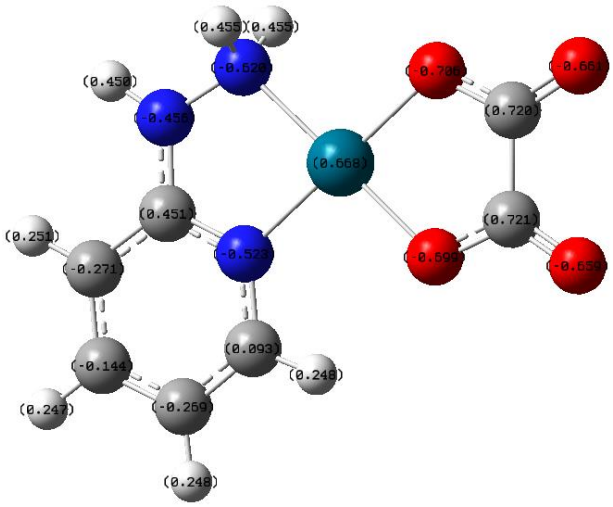

Figure 1. The optimized structure of [Pd(hzpy)(ox)] complex.

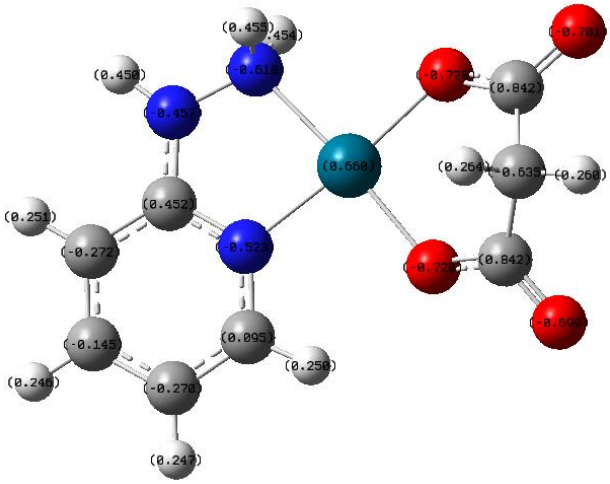

Figure 2. The optimized structure of [Pd(hzpy)(ma)] complex.

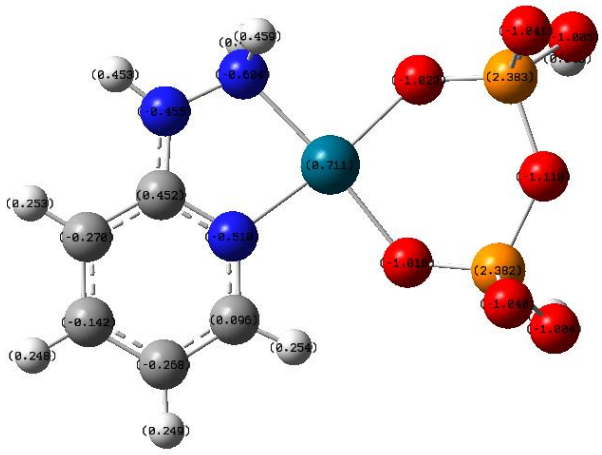

Figure 3. The optimized structure of [Pd(hzpy)(pyph)] complex.

2.4. Evaluation of the antitumor activity

The cytotoxicity testing was performed according to the method reported in the literature [29,30] at the Regional Centre for Mycology and Biotechnology, Al-Azhar University, Cairo, Egypt. The evaluation of the cytotoxic activities was measured against four human cell lines; MCF-7 cells (breast cancer), HepG-2 cells (Hepatocellular carcinoma), PC-3 cells (prostate carcinoma), and HEP-2 (Larynx carcinoma).

2.5. Synthesis of Palladium (II) Complexes.

The three complexes' preparation has been carried out by mixing Na_2PdCl_4 with ligands (hzpy, ox, ma, and pyph) in a 1:1 molar ratio in two steps (Scheme 1). 1.0 mmol (0.294 g) of Na_2PdCl_4 was mixed with 1.0 mmol (0.182 g) of 2-hydrazinopyridine in 30 ml ethanol while stirring at room temperature. 1.0 mmol of the secondary ligand (0.126 g of $H_2C_2O_4$, 0.104 g of $H_4C_3O_4$, and 0.446 g) of $Na_4O_7P_2.10H_2O$) was then added and the mixture was adjusted to pH 3.5 and 4 hours. The solid was precipitated and separated by filtration. The filtered complex was washed thoroughly with hot ethanol. Then with diethyl ether, the solid complex was dried under vacuum and subjected to analysis.

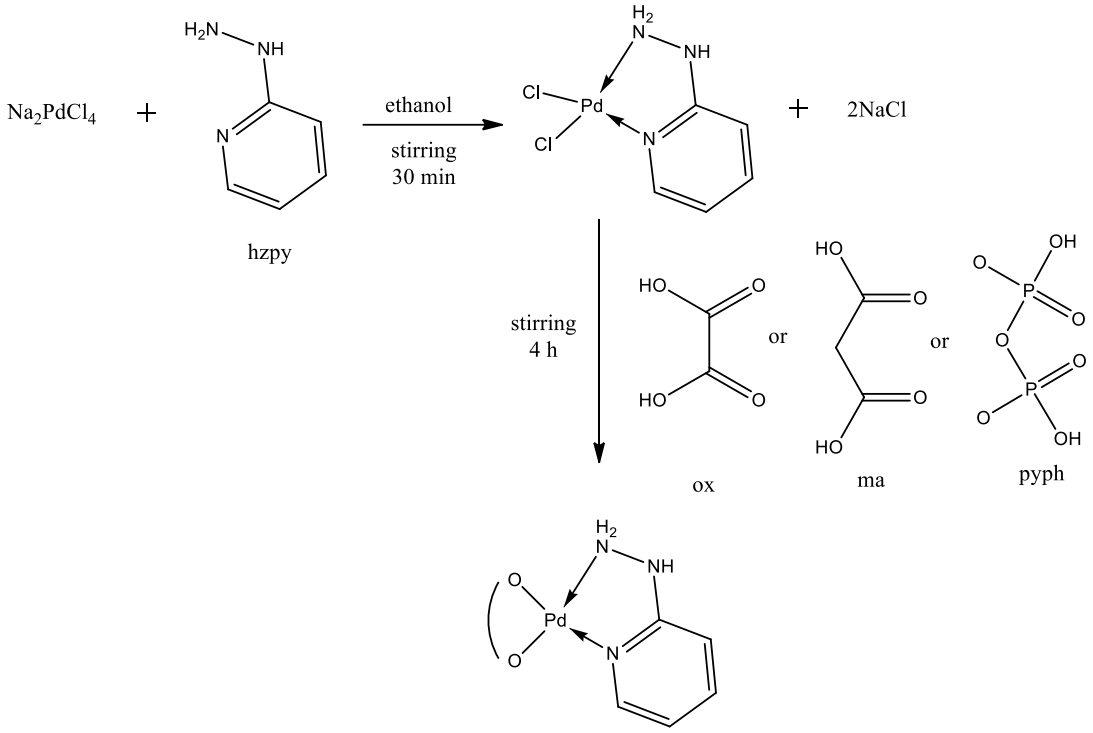

Scheme 1. Preparation of palladium complexes.

[Pd(hzpy)(ox)] complex (1): Yield of 0.236 g (78%). Found: C, 27.46; H, 2.35; N, 12.65. Anal. Calc. for $C_7H_7N_3PdO_4$: C, 27.70; H, 2.32; N, 13.84. IR (KBr, cm^{-1}) υ: 3274 (s), 3159 (s), 1631 (s), 1249 (m), 1188 (s), 763 (s), 532 (w) and 466 (w). ^{1}H-NMR [δ, ppm] (DMSO-d_6): aromatic protons of hzpy ligand (6.69 - 8.38, m, 3H), N-H and NH_2 groups (6.70, m, 3H). FAB-MS: m/z = 302 (M^+-H). UV-Vis: 310, 380, 510, 690 and 715 nm.

[Pd(hzpy)(ma)] complex (2): Yield of 0.26 g (82%). Found: C, 29.45; H, 2.46; N, 12.56. Anal. Calc. for $C_8H_9N_3O_4Pd$: C, 30.25; H, 2.86; N, 13.23. IR (KBr, cm^{-1}) υ: 3274 (s), 3159 (s), 1627 (s), 1284 (m), 1188 (s), 763 (s), 528 (m) and 435 (w). ^{1}H-NMR [δ, ppm] (DMSO-d_6): CH_2 of malonate ligand (3.46, s 2H), aromatic protons of hzpy ligand (6.68 - 8.38, m, 3H), N-H and NH_2 groups (6.69, m, 3H). FAB-MS: m/z = 317 (M^+). UV-Vis: 310, 390, 510, 680 and 720 nm.

[Pd(hzpy)(pyph)] complex (3): Yield of 0.31 g (80%). Found: C, 15.56; H, 2.45; N, 11.35. Anal. Calc. for $C_5H_9N_3P_2Pd$: C, 15.34; H, 2.32; N, 10.79. IR (KBr, cm^{-1}) υ: 3274 (s), 3155 (s), 1249 (w), 1188 (s), 763 (s), 532 (m) and 470 (w). ^{1}H-NMR [δ, ppm] (DMSO-d_6): aromatic protons of hzpy ligand (6.68 - 8.38, m, 3H), N-H and NH_2 groups (6.68, m, 3H). FAB-MS: m/z = 386 (M^+-5H). UV-Vis: 310, 390, 560 and 720 nm.

3. Results and Discussion

3.1. Characterization of palladium complexes.

3.1.1. Infrared spectra.

The IR spectral data of the complexes are tabulated in Table 1. The N-H stretching peaks of the amino group of hzpy ligand were found at 3305 and 3259 cm^{-1} in the spectrum of hzpy ligand (Figure S1) have been appeared in the spectrum of the complex as two strong peaks and being shifted to lower frequencies, upon complex formation, at 3274 and 3159 cm^{-1} indicating the participation of the NH_2 group in coordination (Figure 4). There was a shift to higher frequencies in the deformation vibrations as well at 1249 cm^{-1} (ρt NH_2), 1188 cm^{-1} (ρwNH_2), and 763 cm^{-1} (ρrNH_2), also suggesting that the chelation was through the amino group (Table 1). The calculated deformation vibrations appeared at 1280, 1144, and 763 cm^{-1} with relative errors between -3.7 to 2.5 %. The pyridyl ring's involvement in the chelate formation was confirmed by observing the in-plane and out-of-plane ring deformations at 729 and 474 cm^{-1}, respectively [31]. It is worth noting the experimental and theoretical values of the vibrations were close with low relative error percentages (Figures 4, 5, and Table 1). The band due (υC=O) appeared at 1631 cm^{-1} and the calculated value 1640 with a relative error of 0.6 %. The complex spectrum also showed additional peaks at 532 and 420 cm^{-1} assigned to M-O and M-N bonds, respectively [32, 33].

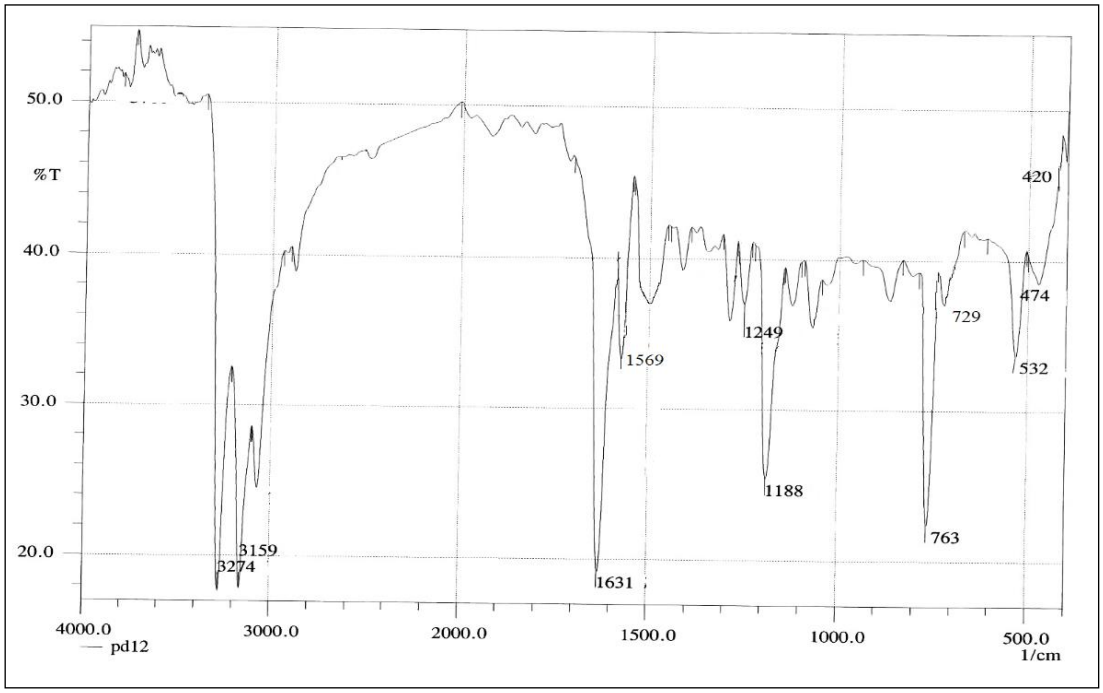

Figure 4. Experimental IR spectrum of [Pd(hzpy)(ox)] complex.

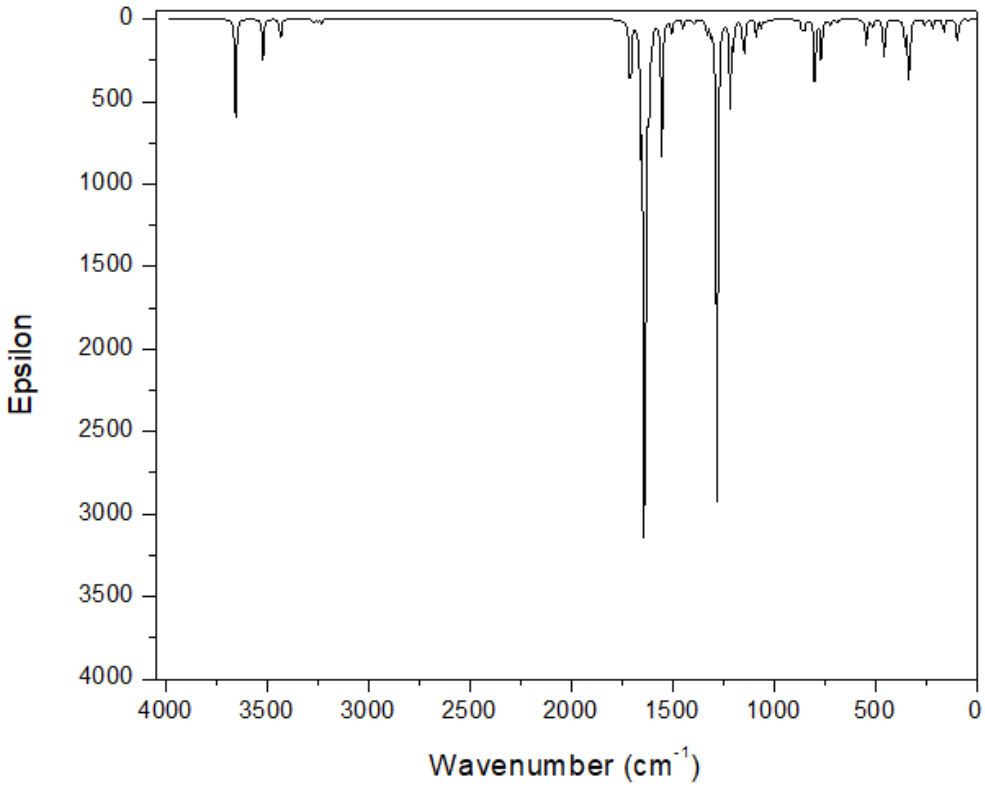

Figure 5. Theoretical IR spectrum of [Pd(hzpy)(ox)] complex.

The infrared spectrum of [Pd(hzpy)(ma)] complex, Figure 6, displayed a similar pattern as the [Pd(hzpy)(ox)] complex. The chelation was through the amnio group, and the pyridyl ring was confirmed through a shift in the N-H stretching and through the in-plane and out-of-plane ring deformations, respectively.

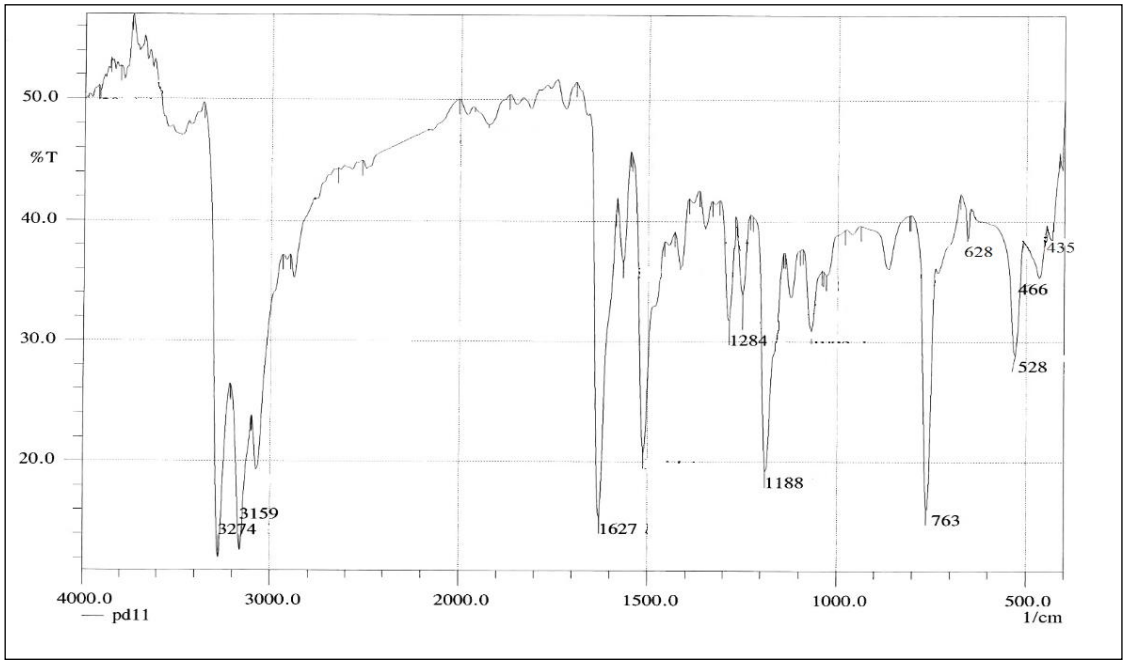

Figure 6. Experimental IR spectrum of [Pd(hzpy)(ma)] complex.

The N-H stretching peaks of the amino group of hzpy were found at 3305 and 3259 cm^{-1} in the spectrum of hzpy ligand (Figure S1; Supplementary materials) that appeared in the spectrum of the complex as two strong peaks and were shifted to lower frequencies at 3274 and 3159 cm^{-1}. Furthermore, the coordination through the NH_2 group was also suggested via

the higher shift of its deformation vibrations observed at 1284 cm^{-1} (ρt NH_2), 1188 cm^{-1} (ρwNH_2), and 763 cm^{-1} (ρrNH_2) (Table 1). The calculated deformation vibrations appeared at 1304, 1144, and 720 cm^{-1} with a relative error between -5.6 to 1.7 %. The pyridyl ring's nitrogen was also supported by observing the in-plane and out-of-plane ring deformations at 628 and 466 cm^{-1}, respectively [31]. The calculated error percentages between the theoretical and experimental spectra were relatively low (Figures 6, 7, and Table 1). The band due (υC=O) appeared at 1627 cm^{-1} and the calculated value 1600 with a relative error of -1.7 %. The complex spectrum showed additional peaks at 528 and 435 cm^{-1} assigned to M-O and M-N bonds, respectively [32, 34].

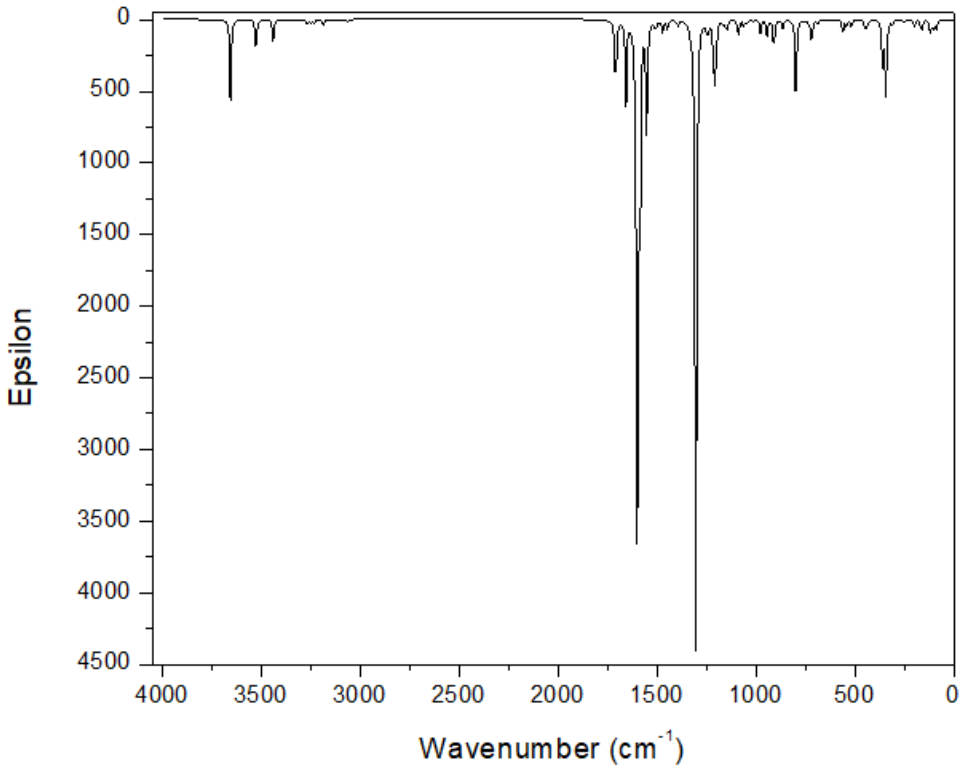

Figure 7. Theoretical IR spectrum of [Pd(hzpy)(ma)] complex.

The IR spectra of the [Pd(hzpy)(pyph)] complex are shown in Figure 8. The N-H stretching peaks of the amino group of hzpy (Figure S1) appeared in the complex spectrum as two strong peaks and were shifted to the lower frequency at 3274 and 3155 $cm^{-1,}$ indicating the participation of the NH_2 group in coordination. The coordination of the NH_2 groups has also been confirmed from the shift of its deformation vibrations (ρtNH_2, ρwNH_2, and ρrNH_2) to higher frequencies at 1249, 1188, and 763 cm^{-1}, respectively (Table 1). The theoretical deformation vibrations appeared at 1304, 11,44 and 720 cm^{-1}, with the relative error between -7.1 to -2.0 %. Generally, the complex's theoretical vibrational spectral data were in good agreement with the corresponding experimental ones (Figure 8, 9, and Table 1). The pyridyl ring's involvement was also supported by the observation of the in-plane and out-of-plane ring deformations at 634 and 470 cm^{-1}, respectively [31]. The band due(υP-O-P) and (υP=O) appeared at 1110 $cm^{-1}$and 921 cm^{-1} in spectrum of the ligand; Figure 8 was found as a small peak, shifted to a lower frequency in the spectrum of the complex at 867 cm^{-1} indicating the coordination of pyph was through the two oxygen atoms. The complex spectrum also exhibited two peaks at 532 and 470 cm^{-1} reflected the M-O and M-N bond's vibration, respectively [32, 34].

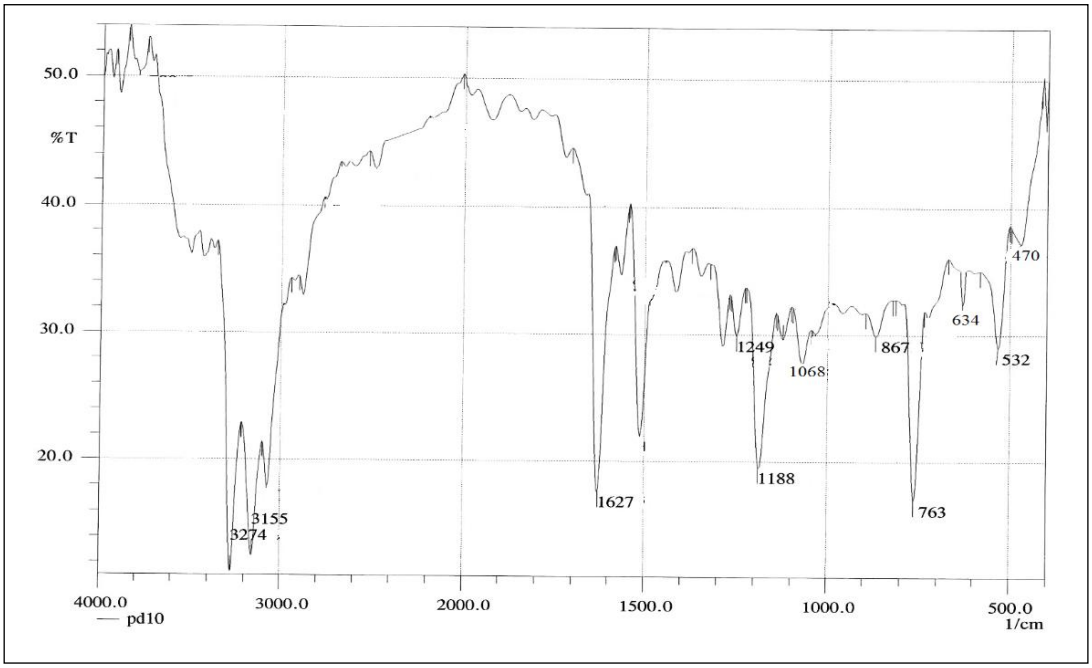

Figure 8. Experimental IR spectrum of [Pd(hzpy)(pyph)] complex.

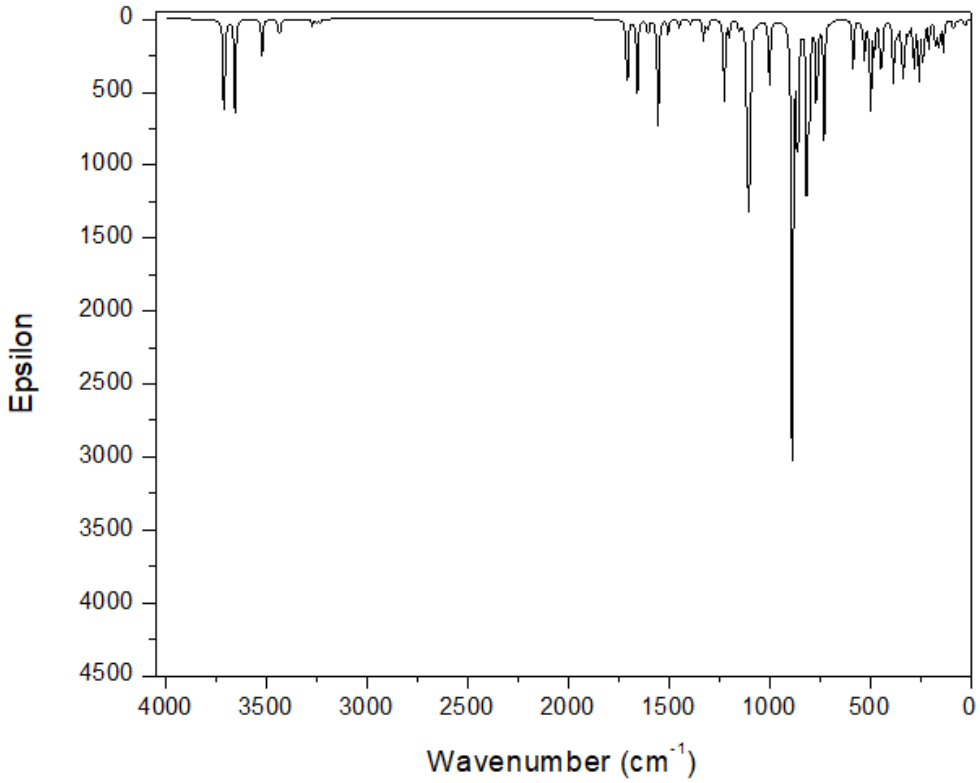

Figure 9. Theoretical IR spectrum of [Pd(hzpy)(pyph)] complex.

Table 1. Characteristic calculated and observed vibrational frequencies cm^{-1} of the palladium complexes

Complex	Obsd	Calcd	Relative error	Assignment
[Pd(hzpy)(ox)]	3274	3520	7.5	υ(NH_2)
	3159	3440	8.9	υ(NH_2)
	1631	1640	0.6	υ(C=O)
	1249	1280	2.5	(ρt NH_2)
	1188	1144	-3.7	(ρwNH_2)
	763	768	0.7	(ρrNH_2)
	532	544	2.3	υ(M-O)
	420	456	8.6	υ(M-N)
[Pd(hzpy)(ma)]	3274	3528	7.8	υ(NH_2)
	3159	3440	8.9	υ(NH_2)

Complex	Obsd	Calcd	Relative error	Assignment
	1627	1600	-1.7	υ(C=O)
	1284	1304	1.6	(ρt NH_2)
	1188	1144	-3.7	(ρwNH_2)
	763	720	-5.6	(ρrNH_2)
	528	560	6.1	υ(M-O)
	435	448	3.0	υ(M-N)
[Pd(hzpy)(pyph)]	3274	3520	7.5	υ(NH_2)
	3155	3432	8.8	υ(NH_2)
	1249	1224	-2.0	(ρt NH_2)
	1188	1104	-7.1	(ρwNH_2)
	1110	1104	-0.5	(υP-O-P)
	921	912	-1.0	(υP=O)
	763	728	-4.6	(ρrNH_2)
	532	504	-5.3	υ(M-O)
	470	448	-4.7	υ(M-N)

3.1.2. ^{1}HNMR spectra.

The NMR spectra confirmed the diamagnetic properties of the three palladium complexes. In the case of [Pd(hzpy)(ox)] complex, the aromatic protons of hzpy ligand were observed as a multiplet at (6.69 - 8.38, m, 3H) in addition to the protons of the N-H and NH_2 groups which were appeared at (6.70, m, 3H). The same peaks appeared almost at the same chemical shifts for [Pd(hzpy)(pyph)] complex; aromatic protons of hzpy ligand (6.68 - 8.38, m, 3H), N-H, and NH_2 groups (6.68, m, 3H). [Pd(hzpy)(ma)] complex exhibited the same peaks in the same regions; aromatic protons of hzpy ligand (6.68 - 8.38, m, 3H), N-H, and NH_2 groups (6.69, m, 3H) in addition to the methylene group of the malonate ligand which appeared as a singlet at (3.46, s, 2H).

3.1.3. Mass spectra.

The mass spectral data of the three palladium complexes are summarized in Table 2. The mass spectrum of [Pd(hzpy)(ox)] complex (M. wt. = 303.57) displayed the parent peak at m/z = 302 (M^+ - H) in addition to a peak at m/z=110 that is assigned to (hzpy) ligand and a peak at m/z=140 assigned to (PdO_2) compound. The mass spectrum of [Pd(hzpy)(ma)] complex (M. wt. = 317.59) showed a peak at m/z = 317 assigned to the parent peak (M^+). The spectrum showed two peaks at m/z=109 and at m/z=150, which corresponded to hzpy ligand and $PdCO_2$. The mass spectrum of [Pd(hzpy)(pyph)] complex (M. wt. = 391.51) gave a parent peak at m/z = 386 (M^+ - $5H^+$), peak at m/z=109 assigned to (hzpy) and peak at m/z=156 assigned to (P_2O_5). The palladium oxide (PdO) appeared in the three palladium spectra at m/z = 122.

Table 2. Important mass data of palladium complexes.

Complex	Molar mass	m/z Values
[Pd(hzpy)(ox)]	303.57	302, 301, 215, 140, 134, 109, 108, 106, 104.
[Pd(hzpy)(ma)]	317.59	317, 312, 231, 150, 125, 118, 117, 109, 105, 104
[Pd(hzpy)(pyph)	391.51	386, 231, 175, 156, 126, 119, 110, 109, 104, 94

3.1.4. UV-Vis spectra.

The three complexes' UV-Vis spectra were recorded in the visible region, and the electronic transition and their assignments are listed in Table 3. The absorption spectrum of [Pd(hzpy)(ox)] complex (Figure 10) displayed a broadband in 280-350 nm region with maxima at 310 nm, which was assigned to the π-π* transition within the hzpy ligand. The n-π* transition overlapped with MLCT. Both appeared as a shoulder at 380 nm [35, 36]. The *d-d* transitions expected for square planar geometry were observed at 510, 690, and 715 nm, which may be

assigned to $^1A_{1g} \rightarrow {}^1E_g$, $^1A_{1g} \rightarrow {}^1A_{2g}$ and $^1A_{1g} \rightarrow {}^3A_{2g}$; respectively [37]. The same pattern was also observed in the other two complexes; [Pd(hzpy)(ma)] and [Pd(hzpy)(pyph)]. The intra-ligand transitions within the hzpy ligand were in the same region 280-350 nm range with maxima at 310 nm. MLCT transitions appeared as a shoulder at 390 nm that was overlapped with n-π* electronic transition in two spectra. [35, 36] The *d-d* transitions in the case of [Pd(hzpy)(ma)] complex appeared between 510 - 720 nm (Figure 11) and between 560 - 720 nm for [Pd(hzpy)(pyph)] complex (Figure 12) [37].

Table 3. The calculated electronic excitations based on TD-DFT/B3LYP/SDD method and the corresponding experimental absorption values of the three palladium complexes.

Excitation (eV)	Wavelength (nm)	Oscillator strength	Major transition(s) (% contribution)		Character	Exp.
[Pd(hzpy)(ox)]						
4.396	282	0.159	60 -> 62 57 -> 64 53 -> 64	(68 %) (7 %) (6 %)	π->π*	310
3.434	361	0.001	58 -> 61 50 -> 61	(53 %) (14 %)	d-d π->π*	380
2.850	435	0.001	56 -> 61 58 -> 61	(63 %) (30 %)	d-d MLCT	460
[Pd(hzpy)(ma)]						
4.412	281	0.123	64 -> 66	(63 %)	π->π*	310
3.212	386	0.0001	60 -> 65 62 -> 65	(48 %) (42 %)	d-d π->π*	380
2.924	424	0.0002	63 -> 65 64 -> 65	(63 %) (18 %)	d-d MLCT	485
[Pd(hzpy)(pyph)]						
4.459	278	0.121	81 -> 83 82 -> 83	(69 %) (14 %)	π->π*	310
3.244	382	0.0002	78 -> 83 82 -> 83	(49 %) (27 %)	d-d π->π*	365
2.658	466	0.0009	82 -> 84 81 -> 84	(63 %) (18 %)	d-d MLCT	-

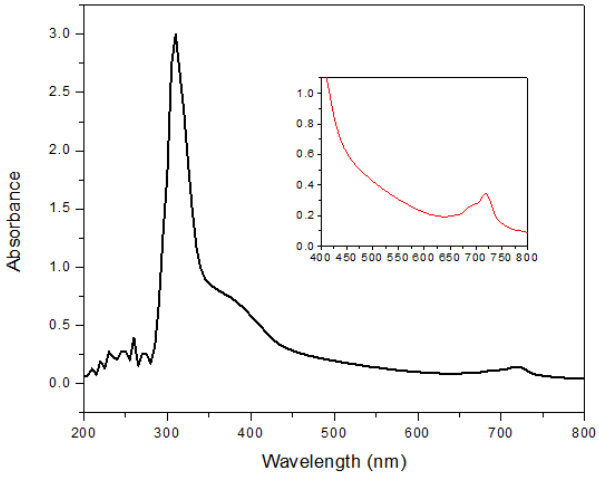

Figure 10. Experimental UV-Vis spectrum of [Pd(hzpy)(ox)] complex.

3.1.5. Magnetic properties.

Magnetic susceptibility measurements also confirmed the diamagnetic nature of the three palladium complexes. Therefore, the three complexes have square planner geometry, and the Pd(II) metal ion center has d^8 configuration e_g^4 a_{1g}^2 b_{2g}^2. Based on different analysis techniques (spectral and magnetic), the hzpy coordinated via the amino group and the pyridyl ring's nitrogen atom. Oxalate, malonate, and pyrophosphate act as bidentate through their oxygen atoms.

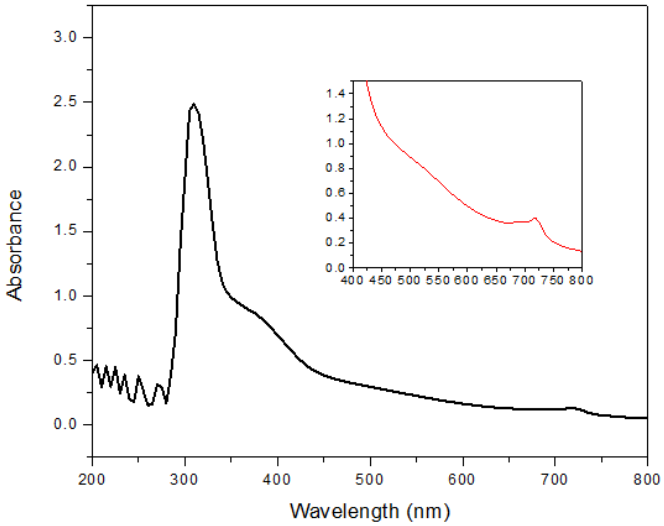

Figure 11. Experimental UV-Vis spectrum of [Pd(hzpy)(ma)] complex.

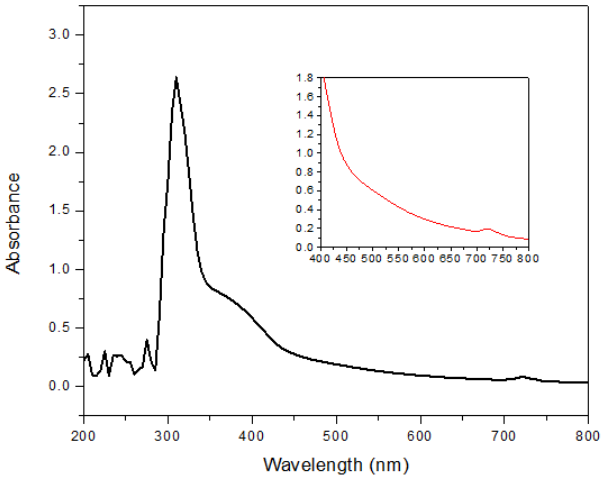

Figure 12. Experimental UV-Vis spectrum of [Pd(hzpy)(pyph)] complex.

3.1.6. Thermal analysis.

The three palladium complexes' thermal properties were investigated through TGA and DTG plots (Figure S2–S4; Supplementary materials).). The temperatures of decomposition and the corresponding mass losses of species are given in (Table 4). The thermal decomposition steps of each complex are shown in Schemes 2 - 4. TGA and DTG plots (Figure S2; Supplementary materials).) of [Pd(hzpy)(ox)] complex showed that the complex decomposed through two steps; Scheme 2. The first step was between 451 - 680 K and reflected the loss of 54.3 % of the sample (54.4 % calc.), such loss assigned to the elimination of hzpy ligand ($C_5H_3N_3$) and 2CO species (mass = 165; m/z = 140).

Table 4. Thermo Analytical data of palladium complex.

Complexes	TG range (K)	DTA_{max} (K)	Mass loss found (calcd. %)	Assignment of the removed species	Metallic residue found (cal.%)
[Pd(hzpy)(ox)]	471-780 1102-1175	483 1120	54.3, (54.4) 5.2, (5.1)	$C_5H_7N_3$, 2CO $1/2O_2$	PdO 40.5; (40.2)
[Pd(hzpy)(ma)]	464-754 1076-1177	473 1156	52.7; (52.6) 8.01; (8.8)	$C_5H_9N_3$, 2CO CO	PdO 38.5; (38.4)
[Pd(hzpy)(pyph)]	431-531 531-1213	478 1156	30.07; (32.6) 37.3; (36.5)	$C_5H_7N_3$, H_2O P_2O_5	PdO 30.1; (31.3)

The second one (1102 - 1175 K) was due to the loss of 5.2 % (5.1 % calc.) could be attributed to the loss of 1/2O_2 species. The palladium oxide (PdO) (mass = 122) 40.5 %, was the residue at the end of the analysis (40.2 % calc).

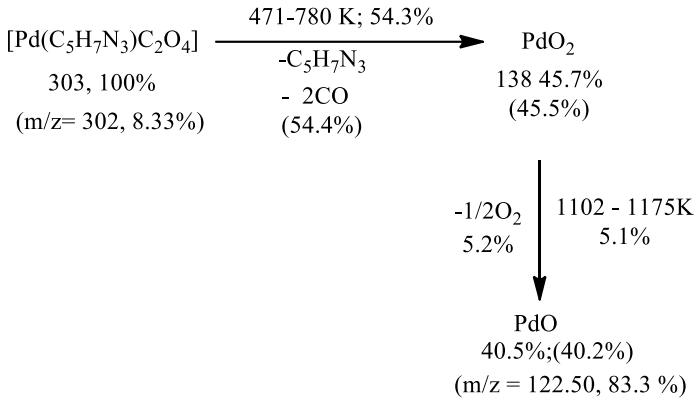

Scheme 2. Thermal decomposition of [Pd(hzpy)(ox)] complex.

The thermal analysis of the [Pd(hzpy)ma] complex (Figure S3; Supplementary materials) involves two decomposition steps, Scheme 3, at 464 – 753 and 1176 - 1177 K. The decomposition also started with the removal of (hzpy) $C_5H_7N_3$ in addition to 2CO species (mass = 165; m/z = 167.2). The second decomposition step was due to the removal of 8.01 % (8.8 % calc.), which may be attributed to the loss of CO. Palladium oxide PdO (mass = 122; m/z = 122.6) was the only residue at the end of the analysis; 38.5 %, (38.4 % calc.).

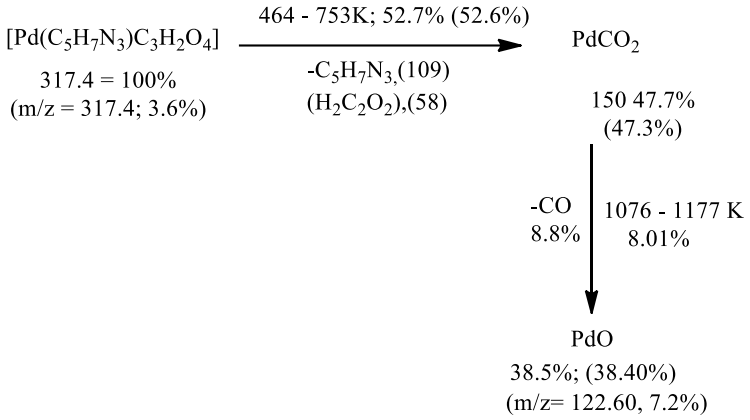

Scheme 3. Thermal decomposition of [Pd(hzpy)(ma)] complex.

TGA plot (Figure S4; Supplementary materials) of [Pd(hzpy)pyph] complex showed that the decomposition included two steps; Scheme 4. The first decomposition step (431 – 531 K), resulted from removing the hzpy and water groups 30.07 % (32.6 % calc.). The second one, the weight loss, was 37.3 % of the sample (36.5 % calc.) due to the loss of P_2O_5 compound (mass = 142; m/z = 142.7). PdO 30.1%, (31.3 % calc) was the oxide residue (mass=122; m/z=125.2). The thermodynamic parameters of the decomposition peaks were calculated using Horowitz-Metzger and Coats-Redfern equations [38-43]. The correlation coefficients of the Arrhenius plots of the three complexes' thermal decomposition steps were found to range from 0.81 - 0.97, indicating good fitness of the linear function. Table 5 gives the decomposition temperature ranges, DTG peak temperature, correlation coefficients of the Arrhenius plots, and the thermodynamic parameters. The complexes showed considerable thermal stability, which is reflected from the overall activation energy sum to 678, 981, and 633 kJ mol^{-1} for [Pd(hzpy)(ox)]. [Pd(hzpy)(ma)] and [Pd(hzpy)(pyph)], respectively compared to that of

[Pd(hzpy)Cl_2], which has an overall activation energy of 580 KJ $mol^{-1,}$ reflecting that the former complexes have two chelating agents instead of one as in the latter complex.

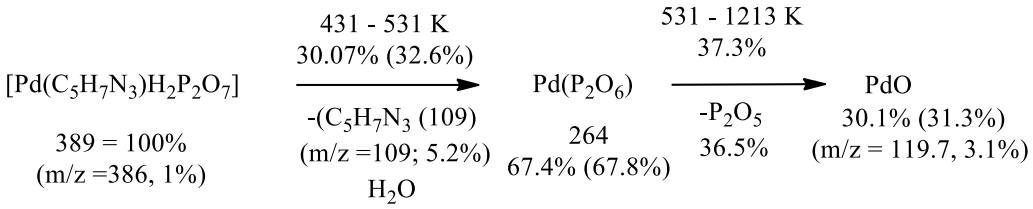

Scheme 4. Thermal decomposition of [Pd(hzpy)(pyph)] complex.

Table 5. Thermodynamic data of the palladium complexes.

Complex	Decomposition temperature (K)	ΔE K J mol^{-1}	R^2	ΔS J K^{-1} mol^{-1}	ΔH K J mol^{-1}	ΔG K J mol^{-1}
[Pd(hzpy)(ox)]	464-753	50	0.81	-177	46	139
	1076-1177	628	0.97	287	618	291
		678		110	664	430
[Pd(hzpy)(ma)]	464-753	42	0.81	-192	38	138
	1076-1177	939	0.96	558	929	292
		981		366	967	430
[Pd(hzpy)(pyph)]	394-822	49	0.90	-181	44	140
	1080-1213	584	0.96	238	574	299
		633		57	618	439

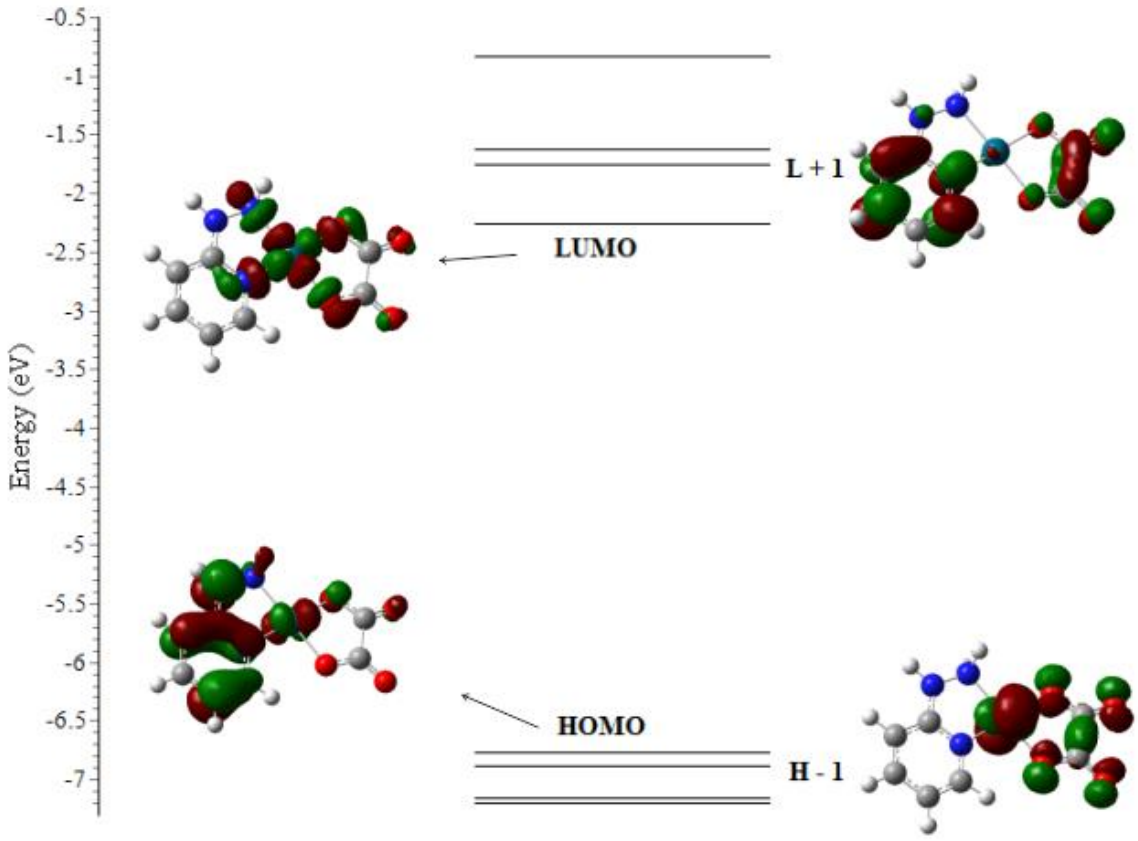

Figure 13. The energy (eV), character, and some contours of the molecular orbitals of [Pd(hzpy)(ox)] complex.

3.2. Theoretical studies.

The optimized geometries of the complexes are given in Figures 1 – 3. Bond lengths and angles surrounding the central palladium ion are reported in Tables S1 - S3; Suplementary materials). The Pd-N and Pd-O bond lengths are within the regular range reported in the literature [16, 44]. TD-DFT investigations calculations were made to study the electronic transitions. Frequency calculations were performed for the optimized geometries. Different

quantum parameters were calculated (frontier energy levels, softness, hardness, electronegativity, chemical potential, and electronic charge) to study the palladium complexes' stability (Table 6) [45-50]. The HOMO - LUMO diagrams of the palladium complexes are shown in Figures 13 - 15, and the energy gaps of [Pd(CPDA)(ox)], [Pd(CPDA)(ma)] and [Pd(CPDA)(pyph)] are equal to 4.51, 4.57 and 4.16 eV, respectively; these energy gaps indicate that the two complexes are stable transition metal complexes [51].

Table 6. Calculated quantum parameters.

Complex	HOMO	LUMO	x	η	σ	pi	ΔE	ω	ΔN_{max}
[Pd(hzpy)(ox)]	-6.77	-2.25	4.51	2.25	0.44	-4.51	4.51	4.51	1.99
[Pd(hzpy)(ma)]	-6.7	-2.15	4.43	2.28	0.43	-4.43	4.57	4.30	1.94
[Pd(hzpy)(pyph)]	-6.85	-2.69	4.77	2.08	0.48	-4.77	4.16	5.47	2.29

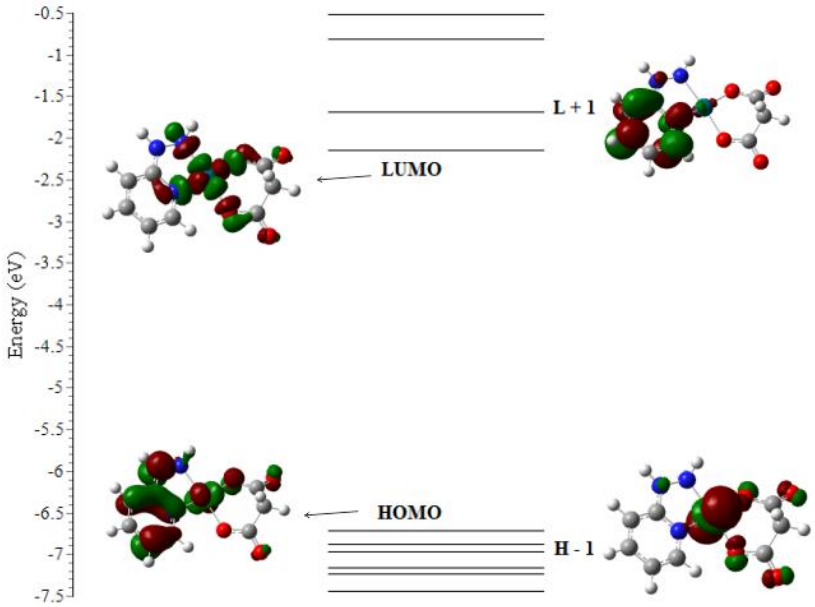

Figure 14. The energy (eV), character, and some contours of the molecular orbitals of [Pd(hzpy)(ma)] complex.

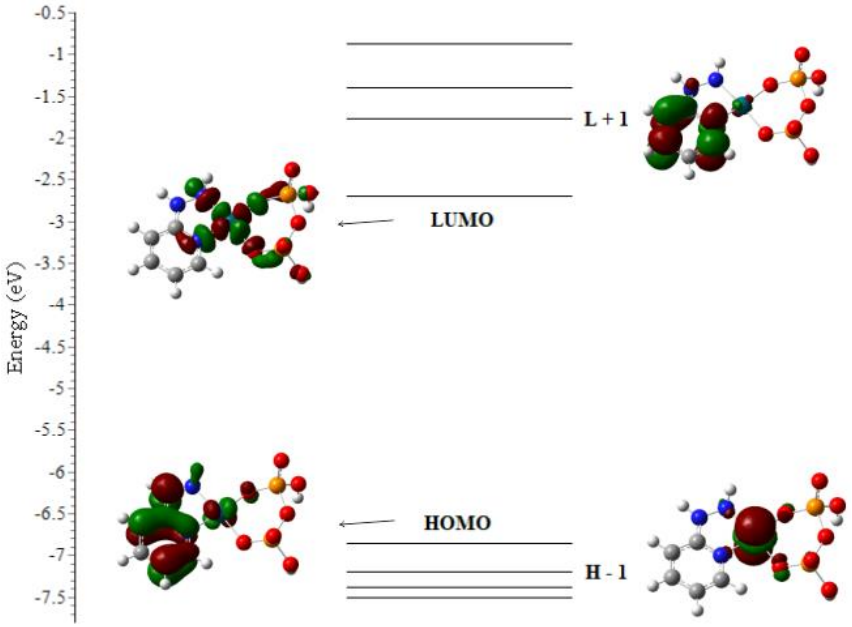

Figure 15. The energy (eV), character, and some contours of the molecular orbitals of [Pd(hzpy)(pyph)] complex.

The three palladium complexes' UV-Vis spectra were studied, and the corresponding electronic transitions were investigated using TDDFT based on the optimized singlet state geometry (square planar) using SDD basis set (Figures S4 – S7; Supplementary materials). In [Pd(hzpy)(ox)] complex, HOMO orbital is localized mainly on π orbitals of hzpy ligand (75 %) in addition to 18 % from *d*-orbital of Pd(II) while H – 1 orbital consists of d-orbital of Pd(II) (65 %). LUMO orbital was constructed from 55 % of *d*-orbital of Pd(II) and 26 % of π orbitals of hzpy ligand. The L + 1 orbital is originated from π orbitals of the hzpy ligand (73 %). Based on TDDFT, the complex exhibited an intense band (λ_{max}) at 282 nm and other peaks at 361 and 435 nm. At 361 nm, the transition was due to *d-d* transitions, MLCT, and n/π->π* of ox ligand. The corresponding transition appeared as a shoulder at 380 nm. The peak appeared at 435 nm resulting from the combination of *d-d* and MLCT ($d\pi_{(Pd)}$-> π^*_{hzpy}).

In [Pd(hzpy)(ma)] complex, HOMO orbital was constructed from 64 % of π orbital of hzpy ligand in addition to 25 % from *d*-orbitals of Pd(II) ion. H – 1 orbital is mainly based on *d*-orbitals of Pd(II) metal (83 %). LUMO is based on d-orbitals of Pd(II) ion (55 %), π orbitals of hzpy (26 %), and ma (18 %) ligands. L + 1 orbital is originated solely from the π orbital of hzpy ligand (97 %). Based on TDDFT, the complex exhibited an intense band (λ_{max}) at 281 nm and other peaks at 386 and 424 nm. At 386 nm, the transition was due to *d-d* transitions, MLCT, and n/π->π* of ma ligand. The corresponding transition appeared as a shoulder at 380 nm. The peak appeared at 424 nm resulting from the combination of *d-d* and MLCT ($d\pi_{(Pd)}$-> π^*_{hzpy}).

In [Pd(hzpy)(pyph)] complex, the frontier orbitals are located mainly on the hzpy ligand. HOMO orbital is constructed from 82 % of π orbital of hzpy ligand, and H – 1 orbital is mainly based on *d*-orbitals of Pd(II) metal (91 %). LUMO is based on *d*-orbitals of Pd(II) ion (53 %), π orbitals of hzpy (27 %), and pyph (21 %) ligands. L + 1 orbital is originated solely from the π orbital of hzpy ligand (97 %). Based on TDDFT, the complex exhibited an intense band (λ_{max}) at 278 nm and other peaks at 382 and 466 nm. At 382 nm, the transition was due to *d-d* transitions, MLCT, and n/π->π* of ma ligand. The corresponding transition appeared as a shoulder at 365 nm. The peak appeared at 466 nm resulting from the combination of *d-d* and MLCT ($d\pi_{(Pd)}$-> π^*_{hzpy}).

Natural Bond Orbital (NBO) calculations [52] were performed at the B3LYP/SDD level of theory. Donations from dinitrogen ligands to Pd(II) exceeded back donations from metal to ligand and the charges on the palladium are lower than the formal + 2 charge; 0.390 for complex with hzpy ligand and Cl ions. The charges on the palladium ions were 0.668, 0.668 and 0.711 for complexes based on hzpy ligand with ox, ma and pyph ligands, respectively. [53] According to the NBO analysis for the palladium complexes, the electronic configurations of the Pd atom are the following: [Pd(hzpy)(ox)] complex: [core] $4d_{xy}$ 1.13937, $4d_{xz}$ 1.97591, $4d_{yz}$ 1.977308, $4d_{x2-y2}$ 1.72177, $4d_{z2}$ 1.96300. [Pd(hzpy)(ma)] complex: [core] $4d_{xy}$ 1.24526, $4d_{xz}$ 1.97022, $4d_{yz}$ 1.89940, $4d_{x2-y2}$ 1.70424, $4d_{z2}$ 1.95074. [Pd(hzpy)(pyph)] complex: [core] $4d_{xy}$ 1.53420, $4d_{xz}$ 1.95535, $4d_{yz}$ 1.87690, $4d_{x2-y2}$ 1.51599, $4d_{z2}$ 1.92823. The total palladium valence populations are 8.77, 8.76 and 8.81 for [Pd(hzpy)(ox)], [Pd(hzpy)(ma)] and [Pd(hzpy)(pyph)] complexes, respectively.

The molecular electrostatic potentials (MEPs) were used to highlight the negative (red) and positive (blue) regions of each complex [54]. The reddish areas were located mainly on the oxalate, malonate, and pyrophosphate ligands (Figures 16 - 18).

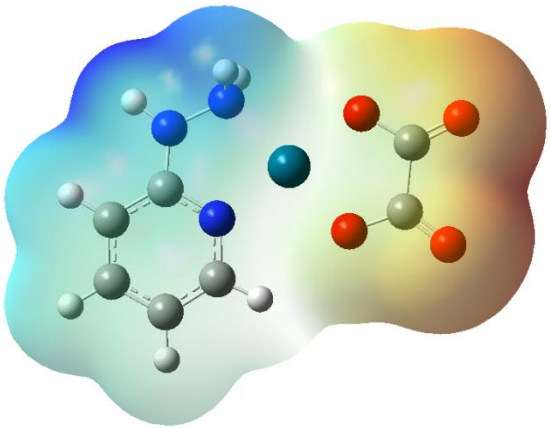

Figure 16. MEP mapping [Pd(hzpy)(ox)] complex.

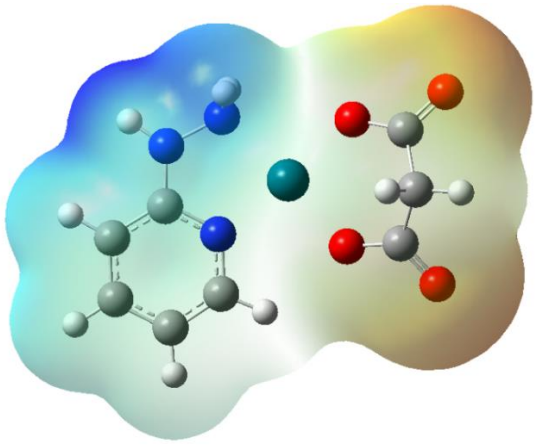

Figure 17. MEP mapping [Pd(hzpy)(ma)] complex.

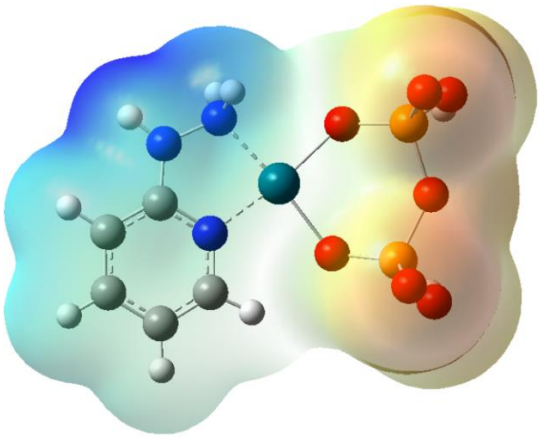

Figure 18. MEP mapping [Pd(hzpy)(pyph)] complex.

3.3. Cytotoxicity.

The *in vitro* cytotoxicity of the three palladium complexes against four cancer cell lines (MCF-7, HEPG-2, PC-3, and HEP-2) was investigated through the literature's method, and the IC_{50} values are tabulated summarized in Table 7. Vinblastine sulfate was used as a standard (Table 7). The relation between the complex concentration and the corresponding surviving cells was plotted to obtain each tumor cell line's survival curve after treatment with each complex (Figures S8 – S11; Supplementary materials). The IC_{50} values were calculated from the graphs of the dose-response curve for each conc. using Graphpad Prism software (San Diego, CA. USA). The IC_{50} values of the [Pd(hzpy)(ox)] complex were relatively low and close

to that of the Vinblastine sulfate. It is worth noting that the three complexes exhibited an excellent performance against PC-3 cell line, the IC_{50} values were: 2.87, 29.5, and 14.9 μg/ml for [Pd(hzpy)(ox)], [Pd(hzpy)(ma)] and [Pd(hzpy)(pyph)], respectively, compared to that of Vinblastine sulfate (42.4 μg/ml). [Pd(hzpy)(ox)] complexes showed the lowest IC_{50} values against the four cancer cell lines, which may be resulted from the formation of the stable species of the complex in contrast to [Pd(hzpy)(ma)] complex, which may suggest a role of the methylene group in such behavior in reducing of the cytotoxic activities.

Table 7. IC_{50} values of the antitumor activities of the palladium complexes.

Complex	HEP-2	PC-3	MCF-7	HEPG-2
Vinblastine sulfate	29.9	42.4	5.9	2.93
[Pd(hzpy)(ox)]	14.2	2.87	6.87	3.39
[Pd(hzpy)(ma)]	55.8	29.5	46.9	28.4
[Pd(hzpy)(pyph)]	41.4	14.9	30.7	21.3

4. Conclusions

Three water-soluble Pd(II) complexes based on 2-hydrazinopyridine were prepared and characterized. The 2-hydrazinopyridine ligand was coordinated via the two amino groups. The malonate, oxalate, and pyrophosphate acted as a bidentate ligand and were coordinated via oxygen atoms. Spectroscopic and magnetic analyses conformed that the palladium complexes were square planar and diamagnetic. The thermal stability of the complexes was studied. DFT calculations were performed to study the theoretical properties of the complexes in the gas phase. The theoretical investigations also suggested that the complexes were stable. [Pd(hzpy)(ox)] complexes showed the lowest IC_{50} values against the four cancer cell lines, which may be resulted from the formation of the stable species of the complex. The three complexes exhibited enhanced cytotoxic activity against PC-3 cancer cell lines than the standard (Vinblastine sulfate). The IC50 values of the complexes were 2.87, 29.5, 14.9 and 42.4 for [Pd(hzpy)(ox)], [Pd(hzpy)(ox)], [Pd(hzpy)(ox)] and Vinblastine sulfate, respectively. Further investigations are required for correlating the antitumor activities and structure of the complexes.

Funding

This research received no external funding

Acknowledgments

This research has no acknowledgment.

Conflicts of Interest

No conflict of interest as declared by the authors.

References

1. Soliman, A.A.; Amin, M.A.; Sayed, A.M.; Abou-Hussein, A.A.A.; Linert, W. Cobalt and copper complexes with formamidine ligands: Synthesis, crystal X-ray study, DFT calculations and cytotoxicity. *Polyhedron* **2019**, *161*, 213-221, https://doi.org/10.1016/j.poly.2018.12.020.
2. Espino, J.; Fernández-Delgado, E.; Estirado, S.; de la Cruz-Martinez, F.; Villa-Carballar, S.; Viñuelas-Zahínos, E.; Luna-Giles, F.; Pariente, J.A. Synthesis and structure of a new thiazoline-based palladium(II) complex that promotes cytotoxicity and apoptosis of human promyelocytic leukemia HL-60 cells. *Sci. Rep.* **2020**, *10*, 16745, https://doi.org/10.1038/s41598-020-73488-0.

3. Oliveira, C.G.; Romero-Canelón, I.; Coverdale, J.P.C.; Maia, P.I.S.; Clarkson, G.J.; Deflon, V.M.; Sadler, P.J. Novel tetranuclear PdII and PtII anticancer complexes derived from pyrene thiosemicarbazones. *Dalton Transactions* **2020**, *49*, 9595-9604, https://doi.org/10.1039/D0DT01133A.
4. Carneiro, T.J.; Martins, A.S.; Marques, M.P.M.; Gil, A.M. Metabolic Aspects of Palladium(II) Potential Anti-Cancer Drugs. *Front. Oncol.* **2020**, *10*, 2218, https://doi.org/10.3389/fonc.2020.590970.
5. Bellemin-Laponnaz, S. N-Heterocyclic Carbene Platinum Complexes: A Big Step Forward for Effective Antitumor Compounds. *Eur. J. Inorg. Chem.* **2020**, *2020*, 10-20, https://doi.org/10.1002/ejic.201900960.
6. Tokgun, O.; Karakas, D.E.; Tan, S.; Karagür, E.R.; İnal, B.; Akca, H.; Durap, F.; Baysal, A.; Aydemir, M. Novel ruthenium and palladium complexes as potential anticancer molecules on SCLC and NSCLC cell lines. *Chemical Papers* **2020**, *74*, 2883-2892, https://doi.org/10.1007/s11696-020-01129-x.
7. Sajadiyeh, E.; Tabatabaee, M.; Seifati, S.M.; Derikvand, Z. Cytotoxic Effect of Palladium(II) Complex with 4-Amino-5-Methyl-2H-1,2,4-Triazole-3(4H)-Thione Ligand on MCF-7 Cell Line. *Pharm. Chem. J.* **2020**, *54*, 145-147, https://doi.org/10.1007/s11094-020-02171-5.
8. Omondi, R.O.; Bellam, R.; Ojwach, S.O.; Jaganyi, D.; Fatokun, A.A. Palladium(II) complexes of tridentate bis(benzazole) ligands: Structural, substitution kinetics, DNA interactions and cytotoxicity studies. *J. Inorg. Biochem.* **2020**, *210*, 111156, https://doi.org/10.1016/j.jinorgbio.2020.111156.
9. Mbugua, S.N.; Sibuyi, N.R.S.; Njenga, L.W.; Odhiambo, R.A.; Wandiga, S.O.; Meyer, M.; Lalancette, R.A.; Onani, M.O. New Palladium(II) and Platinum(II) Complexes Based on Pyrrole Schiff Bases: Synthesis, Characterization, X-ray Structure, and Anticancer Activity. *ACS Omega* **2020**, *5*, 14942-14954, https://doi.org/10.1021/acsomega.0c00360.
10. Bošković, M.; Franich, A.A.; Rajković, S.; Jovanović, M.; Jurisević, M.; Gajović, N.; Jovanović, M.; Arsenijević, N.; Jovanović, I.; Živković, M.D. Potential Antitumor Effect of Newly Synthesized Dinuclear1,5-Naphthyridine-Bridging Palladium(II) Complexes. *ChemistrySelect* **2020**, *5*, 10549-10555, https://doi.org/10.1002/slct.202002350.
11. Budzisz, E.; Miernicka, M.; Lorenz, I.-P.; Mayer, P.; Krajewska, U.; Rozalski, M. Synthesis and X-ray structure of platinum(II), palladium(II) and copper(II) complexes with pyridine–pyrazole ligands: Influence of ligands' structure on cytotoxic activity. *Polyhedron* **2009**, *28*, 637-645, https://doi.org/10.1016/j.poly.2008.12.013.
12. Czarnomysy, R.; Radomska, D.; Muszyńska, A.; Hermanowicz, J.M.; Prokop, I.; Bielawska, A.; Bielawski, K. Evaluation of the Anticancer Activities of Novel Transition Metal Complexes with Berenil and Nitroimidazole. *Molecules* **2020**, *25*, https://doi.org/10.3390/molecules25122860.
13. Alinaghi, M.; Karami, K.; Shahpiri, A.; nasab, A.K.; Momtazi-Borojeni, A.A.; Abdollahi, E.; Lipkowski, J. A Pd(II) complex derived from pyridine-2-carbaldehyde oxime ligand: Synthesis, characterization, DNA and BSA interaction studies and in vitro anticancer activity. *J. Mol. Struct.* **2020**, *1219*, 128479, https://doi.org/10.1016/j.molstruc.2020.128479.
14. Omondi, R.O.; Ojwach, S.O.; Jaganyi, D. Review of comparative studies of cytotoxic activities of Pt(II), Pd(II), Ru(II)/(III) and Au(III) complexes, their kinetics of ligand substitution reactions and DNA/BSA interactions. *Inorg. Chim. Acta* **2020**, *512*, 119883, https://doi.org/10.1016/j.ica.2020.119883.
15. Jung, Y.; Lippard, S.J. Direct Cellular Responses to Platinum-Induced DNA Damage. *Chem. Rev.* **2007**, *107*, 1387-1407, https://doi.org/10.1021/cr068207j.
16. Małecki, J.G.; Maroń, A. Spectroscopic, structure and DFT studies of palladium(II) complexes with pyridine-type ligands. *Transition Met. Chem.* **2011**, *36*, 297-305, https://doi.org/10.1007/s11243-011-9469-z.
17. Ferraz, K.S.O.; Ferandes, L.; Carrilho, D.; Pinto, M.C.X.; Leite, M.d.F.; Souza–Fagundes, E.M.; Speziali, N.L.; Mendes, I.C.; Beraldo, H. 2-Benzoylpyridine-N(4)-tolyl thiosemicarbazones and their palladium(II) complexes: Cytotoxicity against leukemia cells. *Biorg. Med. Chem.* **2009**, *17*, 7138-7144, https://doi.org/10.1016/j.bmc.2009.08.063.
18. Islami-Moghaddam, M.; Mansouri-Torshizi, H.; Divsalar, A.; Saboury, A.A. Synthesis, characterization, cytotoxic and DNA binding studies of diimine Platinum(II) and Palladium(II) complexes of short hydrocarbon chain ethyldithiocarbamate ligand. *Journal of the Iranian Chemical Society* **2009**, *6*, 552-569, https://doi.org/10.1007/BF03246535.
19. Paul A. K., Srivastava T.S., Chavan S. J., Chitnis M.P., Desai S., and Rao K.K., Synthesis, Characterization, Cytotoxic, and DNA Binding Studies of Some Platinum(lI) Complexes of 1,2-Diamine and a-Diimine with 2-Pyridinecarboxylate Anion. *J. Inorg. Biochem.* **1996**, 61, 179-196,
20. de Moura, T.R.; Zanetti, R.D.; Silva, D.E.S.; de Farias, R.L.; Mauro, A.E.; Pereira, J.C.M.; de Souza, A.A.; da Silva Siqueira, F.; de Souza Júdice, W.A.; Lima, M.A.; Rocha, F.V.; Deflon, V.M.; Vieira de Godoy Netto, A. Palladium(ii) complexes bearing 1-iminothiolate-3,5-dimethylpyrazoles: synthesis, cytotoxicity, DNA binding and enzymatic inhibition studies. *New J. Chem.* **2020**, *44*, 19891-19901, https://doi.org/10.1039/D0NJ02825H.
21. Anu, D.; Naveen, P.; Rath, N.P.; Kaveri, M.V. Palladium (II) complexes containing substituted thiosemicarbazones. Synthesis, spectral characterization, X-ray crystallography, biomolecular interactions and in vitro cytotoxicity. *J. Mol. Struct.* **2020**, *1206*, 127703, https://doi.org/10.1016/j.molstruc.2020.127703.
22.. Ayyannan, G.; Mohanraj, M.; Gopiraman, M.; Uthayamalar, R.; Raja, G.; Bhuvanesh, N.; Nandhakumar, R.; Jayabalakrishnan, C. New Palladium(II) complexes with ONO chelated hydrazone ligand: Synthesis,

characterization, DNA/BSA interaction, antioxidant and cytotoxicity. *Inorg. Chim. Acta* **2020**, *512*, 119868, https://doi.org/10.1016/j.ica.2020.119868.
23. Becke, A.D. Density-functional thermochemistry. III. The role of exact exchange. *The Journal of Chemical Physics* **1993**, *98*, 5648-5652, https://doi.org/10.1063/1.464913.
24. Lee, C.; Yang, W.; Parr, R.G. Development of the Colle-Salvetti correlation-energy formula into a functional of the electron density. *Physical Review B* **1988**, *37*, 785-789, https://doi.org/10.1103/PhysRevB.37.785.
25. Chen W-S and Chen Z-R, Quantum chemical study on asymmetric allylation of benzaldehyde in the presence of chiral allylboronate. *J Zhejiang Univ Sci B.* **2005**, *6*(6), 606–610, https://doi.org/10.1631/jzus.2005.B0606.
26. Dikmen, G.; Hür, D. Palladium (II) complex: Synthesis, spectroscopic studies and DFT calculations. *Chem. Phys. Lett.* **2019**, *716*, 49-60, https://doi.org/10.1016/j.cplett.2018.12.018.
27. Al-Azmi, A. Synthesis, crystal analysis and DFT calculations of Ni(II) and Pd(II) complexes of 3,3'-((1,2-phenylenebis(azanediyl))bis(2-oxoethane-2,1-diyl))bis(1-allyl-1H-imidazole-3-ium). *J. Mol. Struct.* **2019**, *1180*, 179-187, https://doi.org/10.1016/j.molstruc.2018.11.043.
28. M. J. Frisch, G. W. T., H. B. Schlegel, G. E. Scuseria, M. A. Robb, J. R. Cheeseman, G. Scalmani, V. Barone, B. Mennucci, G. A. Petersson, H. Nakatsuji, M. Caricato, X. Li, H. P. Hratchian, A. F. Izmaylov, J. Bloino, G. Zheng, J. L. Sonnenberg, M. Hada, M. Ehara, K. Toyota, R. Fukuda, J. Hasegawa, M. Ishida, T. Nakajima, Y. Honda, O. Kitao, H. Nakai, T. Vreven, J. A. Montgomery, Jr., J. E. Peralta, F. Ogliaro, M. Bearpark, J. J. Heyd, E. Brothers, K. N. Kudin, V. N. Staroverov, T. Keith, R. Kobayashi, J. Normand, K. Raghavachari, A. Rendell, J. C. Burant, S. S. Iyengar, J. Tomasi, M. Cossi, N. Rega, J. M. Millam, M. Klene, J. E. Knox, J. B. Cross, V. Bakken, C. Adamo, J. Jaramillo, R. Gomperts, R.E. Stratmann, O. Yazyev, A. J. Austin, R. Cammi, C. Pomelli, J. W. Ochterski, R. L. Martin, K. Morokuma, V. G. Zakrzewski, G. A. Voth, P. Salvador, J. J. Dannenberg, S. Dapprich, A. D. Daniels, O. Farkas, J. B. Foresman, J. V. Ortiz, J. Cioslowski, D. J. Fox *Gaussian 09, Revision C.01*, Gaussian, Inc., Wallingford CT: 2010.
29. Mosmann, T. Rapid colorimetric assay for cellular growth and survival: Application to proliferation and cytotoxicity assays. *J. Immunol. Methods* **1983**, *65*, 55-63, https://doi.org/10.1016/0022-1759(83)90303-4.
30. Riyadh, S.M.; Gomha, S.M.; Mahmmoud, E.A.; Elaasser, M.M. ChemInform Abstract: Synthesis and Anticancer Activities of Thiazoles, 1,3-Thiazines, and Thiazolidine Using Chitosan-Grafted-Poly(vinylpyridine) as Basic Catalyst. *ChemInform* **2015**, *46*, https://doi.org/10.1002/chin.201538150.
31. Soliman, A.A.; Amin, M.A.; El-Sherif, A.A.; Ozdemir, S.; Varlikli, C.; Zafer, C. Synthesis and characterization of novel series of Fe(II)-mixed ligand complexes involving 2,2′-bipyridyl ligand. *Dyes and Pigments* **2013**, *99*, 1056-1064, https://doi.org/10.1016/j.dyepig.2013.08.007.
32. Soliman, A.A.; Khattab, M.M.; Linert, W. Kinetic and characterization studies of iron(II) and iron(III) complex formation reactions with hydrazinopyridine. *J. Coord. Chem.* **2008**, *61*, 2017-2031, https://doi.org/10.1080/00958970701824373.
33. Nakamoto, K., Applications in Inorganic Chemistry. In *Infrared and Raman Spectra of Inorganic and Coordination Compounds*, pp 149-354, https://doi.org/10.1002/9780470405840.ch2.
34. Mautner, F.A., Jantscher, P.V., Fischer, R.C. et al. Syntheses, structural characterization, and thermal behaviour of metal complexes with 3-aminopyridine as co-ligands. *Transit. Met. Chem.* **2020**. https://doi.org/10.1007/s11243-020-00436-2.
35. Samota, M.K.; Seth, G. Synthesis, characterization, and antimicrobial activity of palladium(II) and platinum(II) complexes with 2-substituted benzoxazole ligands. *Heteroat. Chem* **2010**, *21*, 44-50, https://doi.org/10.1002/hc.20578.
36. Al-Khodir, F.A.I.; Abumelha, H.M.A.; Al-Warhi, T.; Al-Issa, S.A. New Platinum(IV) and Palladium(II) Transition Metal Complexes of s-Triazine Derivative: Synthesis, Spectral, and Anticancer Agents Studies. *BioMed Research International* **2019**, *2019*, 9835745, https://doi.org/10.1155/2019/9835745.
37. Park, S.; Kadkin, O.N.; Tae, J.-G.; Choi, M.-G. Photoresponsive palladium(II) complexes with azobenzene incorporated into benzyl aryl ether dendrimers. *Inorg. Chim. Acta* **2008**, *361*, 3063-3068, https://doi.org/10.1016/j.ica.2008.02.023.
38. Horowitz, H.H.; Metzger, G. A New Analysis of Thermogravimetric Traces. *Anal. Chem.* **1963**, *35*, 1464-1468, https://doi.org/10.1021/ac60203a013.
39. Nath, M.; Arora, P. Spectral and Thermal Studies of Cobalt(II), Nickel(II) and Copper(II) Complexes of Schiff Bases Obtained from o-Hydroxyacetophenone and Amino Acids. *Synth. React. Inorg. Met.-Org. Chem.* **1993**, *23*, 1523-1546, https://doi.org/10.1080/15533179308016704.
40. Coats, A.W.; Redfern, J.P. Kinetic Parameters from Thermogravimetric Data. *Nature* **1964**, *201*, 68-69, https://doi.org/10.1038/201068a0.
41. Soliman, A.A.; El-Medani, S.M.; Ali, O.A.M. Thermalstudy of chromium and molybdenum complexes with some nitrogen and nitrogen-oxygendonors ligands. *J. Therm. Anal. Calorim.* **2006**, *83*, 385-392, https://doi.org/10.1007/s10973-005-7009-9.
42. Soliman, A.A.; Taha, A.; Linert, W. Spectral and thermal study on the adduct formation between square planar nickel(II) chelates and some bidentate ligands. *Spectrochimica Acta Part A: Molecular and Biomolecular Spectroscopy* **2006**, 64, 1058-1064, https://doi.org/10.1016/j.saa.2005.09.015.

43. Kirsch - De Mesmaeker A., Lecomte, J. & Kelly, J. Photoreactions of metal complexes with DNA, especially those involving a primary photo-electron transfer. In: Mattay J. (eds) Electron Transfer II. Topics in Current Chemistry, vol 177. Springer, Berlin, Heidelberg. **2005**, 25-76. https://doi.org/10.1007/3-540-60110-4_2.
44. Guelai, A.; Brahim, H.; Guendouzi, A.; Boumediene, M.; Brahim, S. Structure, electronic properties, and NBO and TD-DFT analyses of nickel(II), zinc(II), and palladium(II) complexes based on Schiff-base ligands. *J. Mol. Model.* **2018**, *24*, 301, https://doi.org/10.1007/s00894-018-3839-9.
45. Zhang, X.-M.; Wu, H.-S.; Chen, X.-M. Linear and Helical Chains in Hydrothermally Synthesized Coordination Polymers [Co(bpdc)(H2O)2] and [Ni(bpdc)(H2O)3]·H2O Involving in situ Ligand Synthesis. *Eur. J. Inorg. Chem.* **2003**, *2003*, 2959-2964, https://doi.org/10.1002/ejic.200300060.
46. Jung, E.J.; Lee, U.k.; Koo, B.K. Hydrothermal synthesis and crystal structure of [Co(2,5-pydc)(H2O)2]n·nH2O (2,5-pydc=2,5-pyridinedicarboxylate). *Inorg. Chim. Acta* **2008**, *361*, 2962-2966, https://doi.org/10.1016/j.ica.2008.01.029.
47. Masoudi, M.; Behzad, M.; Arab, A.; Tarahhomi, A.; Rudbari, H.A.; Bruno, G. Crystal structures, DFT calculations and Hirshfeld surface analyses of three new cobalt(III) Schiff base complexes derived from meso-1,2-diphenyl-1,2-ethylenediamine. *J. Mol. Struct.* **2016**, *1122*, 123-133, https://doi.org/10.1016/j.molstruc.2016.05.092.
48. Parr, R.G.; Pearson, R.G. Absolute hardness: companion parameter to absolute electronegativity. *J. Am. Chem. Soc.* **1983**, *105*, 7512-7516, https://doi.org/10.1021/ja00364a005.
49 Geerlings, P.; De Proft, F.; Langenaeker, W. Conceptual Density Functional Theory. *Chem. Rev.* **2003**, *103*, 1793-1874, https://doi.org/10.1021/cr990029p.
50. Parr, R.G.; Szentpály, L.v.; Liu, S. Electrophilicity Index. *J. Am. Chem. Soc.* **1999**, *121*, 1922-1924, https://doi.org/10.1021/ja983494x.
51. Sagdinc, S.; Köksoy, B.; Kandemirli, F.; Bayari, S.H. Theoretical and spectroscopic studies of 5-fluoro-isatin-3-(N-benzylthiosemicarbazone) and its zinc(II) complex. *J. Mol. Struct.* **2009**, *917*, 63-70, https://doi.org/10.1016/j.molstruc.2008.06.033.
52. Mansour, A.M. Coordination behavior of sulfamethazine drug towards Ru(III) and Pt(II) ions: Synthesis, spectral, DFT, magnetic, electrochemical and biological activity studies. *Inorg. Chim. Acta* **2013**, *394*, 436-445, https://doi.org/10.1016/j.ica.2012.08.025.
53. Małecki, J.G. Spectroscopic, structure, and DFT studies of cationic palladium(II) complexes with imidazole derivative ligands. *J. Coord. Chem.* **2013**, *66*, 1561-1573, https://doi.org/10.1080/00958972.2013.784903.
54. Hussain, R.; Saeed, M.; Mehboob, M.Y.; Khan, S.U.; Usman Khan, M.; Adnan, M.; Ahmed, M.; Iqbal, J.; Ayub, K. Density functional theory study of palladium cluster adsorption on a graphene support. *RSC Advances* **2020**, *10*, 20595-20607, https://doi.org/10.1039/D0RA01059F.